MR Flow Quantification Using RACE: Clinical Application to the Carotid Arteries

Harald E. Möller, PhD • Hans-Kristian Klocke, MD • Georg M. Bongartz, MD • Peter E. Peters, MD

Real time MR flow quantification was performed with real time acquisition and evaluation of motion (RACE) in a rigid phantom under steady flow conditions and in the common carotid arteries of 43 subjects aged 24–78 years. Hemodynamic information included the intraluminal velocity distribution during the complete cardiac cycle, the distensibility of the arterial wall, and age-dependent changes of the flow curves. Systolic peak velocities of 51 ± 33 cm/s and time-averaged volume flow rates of 4.3 ± 2.0 ml/s were measured in healthy subjects. Flow rates below 3.0 ml/s and the observation of abnormal flow patterns indicated stenoses greater than 70% in the region of the bifurcation (sensitivity: 83.3%; specificity: 93.7%; accuracy: 71.4%). Improvements may be achieved from a combination with MR angiography, providing both functional and morphologic vascular information noninvasively within one observer-independent examination. MR imaging, therefore, has a strong potential for the diagnosis of critical stenoses in symptomatic patients.

Index terms: Blood, flow dynamics • Carotid arteries, flow dynamics • Carotid arteries, stenosis or obstruction • Phase imaging • Vascular studies • Velocity studies

JMRI 1996; 6:503–512

Abbreviations: A/B = A/B Ratio, ANOVA = analysis of variance, CCA = common carotid artery, DSA = digital subtraction angiography, ECA = external carotid artery, ECST = European Carotid Surgery Trial, ICA = internal carotid artery, MRA = magnetic resonance angiography, NASCET = North American Symptomatic Carotid Endarterectomy Trial, 1D = one-dimensional, PI = pulsatility index, RACE = real time acquisition and evaluation of motion, 2D = two-dimensional, US = ultrasonography, v_{peak} = peak systolic flow velocity, $\langle v \rangle$ = flow velocity averaged over the cardiac cycle, $\langle \dot{V} \rangle$ = volume flow rate averaged over the cardiac cycle.

[1] From the Westfälische Wilhelms-Universität Münster, Institut für Physikalische Chemie, Schloßplatz 4/7, D-48149 Münster, Germany (H.E.M.) and Institut für Klinische Radiologie, Albert-Schweitzer-Str. 33, D-48129 Münster, Germany (H.E.M., H.K.K., G.M.B., P.E.P.). Current address for G.M.B.: Institut für Diagnostische Radiologie, Universität Basel/Kantonsspital, Petersgraben 4, CH-4031 Basel, Switzerland. Received August 14, 1995; revision requested November 6; revision received December 13; accepted January 2, 1996. A portion of this work was presented at the 11th Annual Meeting of the SMRI in San Francisco, CA 1993. **Address reprint requests to** H.E.M.

MOTIONAL EFFECTS ON MR signals have been known since Hahn's basic paper on spin echoes (1). For medical applications, this inherent sensitivity to flow provides an opportunity for noninvasive vascular imaging without the need for contrast agents, and systematic evaluation of MR angiography (MRA) already started one decade ago (2). Among applications of MRA in the evaluation of cerebrovascular disease, the most common may be the assessment of arterial occlusive disease in patients at risk for stroke. Results of the North American Symptomatic Carotid Endarterectomy Trial (NASCET) or the European Carotid Surgery Trial (ECST) have shown that the percentage of proximal internal carotid artery stenosis is of paramount importance in determining who might benefit from endarterectomy (3,4). The idea of using noninvasive imaging techniques to measure such critical stenoses and determine surgical candidates has therefore become more attractive. However, because MR angiography tended to overestimate the degree of stenosis at the carotid bifurcation in most clinical studies, it has been acknowledged that MRA alone cannot currently replace digital subtraction angiography (DSA) for preoperative evaluation of symptomatic patients in general (5,6).

One approach to further improve noninvasive diagnosis of cerebrovascular disease may be a combination of morphologic MRA data with quantitative flow information normally obtained by Doppler ultrasonography (US) in clinical routine (7). Alternatively, the evolution of magnetization in the presence of gradients, ie, the physical basis of MRA, can also be used to provide such functional data from MR imaging (8). Both vascular images and quantitative flow parameters may therefore be obtained observer-independently within one single MR examination. During the past years, the general feasibility to quantify flow velocities and volume flow rates by means of MR imaging techniques has been demonstrated for different blood vessels as well as for the heart and cerebrospinal fluid. However, most of this work has been performed on a research basis, and the potential for clinical use remains to be further evaluated (9).

The variety of MR techniques aimed at quantification of motion may be subdivided into two broad categories, depending either on time-of-flight or phase effects. At present, methods relying on well defined phase shifts, created by the introduction of an appropriate gradient scheme into the imaging sequence (eg, phase mapping [10–14] Fourier flow imaging [15–17]), are the most wide-

spread quantitative MR flow measuring techniques. They enable the investigation of a wide spectrum of velocities with bidirectional flow sensitivity over quite short time scales and without using relaxation time information. Among the variations of phase-mapping methods, a simple approach that can be implemented on ordinary clinical MR scanners is real time acquisition and evaluation of motion (RACE) (18,19). In this technique, one spatial dimension is sacrificed by omitting the time-consuming phase-encoding procedure to speed up the standard phase-mapping experiment. Consequently, real time monitoring of blood flow is achieved by repeated application of the sequence to the same slice, yielding a projective image with one spatial, one temporal, and one velocity dimension. Typically, 30 to 50 measurements can be performed per cardiac cycle, achieving the investigation of the state of motion along the vessels in high temporal resolution without the need for electrocardiographic gating. The general applicability of RACE has been demonstrated for the aorta (19,20), carotid arteries (19), pulmonary arteries (21), vena cava (22), and cerebrospinal fluid dynamics (19,23).

One objective of the present study was to assess the accuracy and reproducibility of the one-dimensional (1D) RACE technique for quantitative flow measurements in a series of phantom experiments. The capability for an in vivo application in clinical routine was then evaluated in a group of patients with well described arterial occlusive disease in the region of the carotid bifurcation. In addition to the general clinical importance of atherosclerosis of the extracranial cerebral vessels, the common carotid arteries are especially suited for this purpose: they are readily accessible to MR flow measurements, even with projective techniques, because relatively few vessels are present at this location; they provide a straight vessel segment in which flow can be expected to be relatively undisturbed under normal conditions; and they provide a large range of velocities during the cardiac cycle. A further objective of our study was to ascertain the possibility of staging pathologies and to define the diagnostic potential of the method.

• METHODS

MR Flow Phantom

A specially designed flow phantom, similar to those applied earlier by other authors (24), was used for experimental calibration and in vitro validation of the RACE technique. It consisted of a pair of straight glass pipes (20 mm inner diameter) of sufficient length (2.5 m upstream from the region of interest) to achieve full development of well defined flow conditions over the total range of velocities under investigation. Additional surrounding cylinders (180 mm length, 50 mm inner diameter) enabled a direct comparison of flowing and stationary fluids. Continuous flow through the pipes was achieved by an electronic pump (GARDENA 1000 e, Kress + Kastner, Ulm, Germany), which was located outside the magnet room and connected to the model with flexible tubing (13 mm inner diameter). Volume flow rates, $\dot{V}$, adjusted by a valve in the influx loop, varied in the range of 8.3 to 220 ml/s with corresponding Reynolds numbers of 530 to 14,000 and were determined using precisely calibrated float flowmeters (SA 20 K, Krohne, Duisburg, Germany). Reynolds numbers were calculated as:

$$\mathrm{Re} = \frac{\bar{v}\, D\, \rho}{\eta} = \frac{4\, \dot{V} \rho}{\pi\, D\, \eta} \qquad (1)$$

Table 1
Frequency of Different Degrees of Carotid Artery Stenosis as Determined from the Combined Results of Clinical History, Ultrasound, Digital Subtraction Angiography, Magnetic Resonance Angiography, and Surgical Approval

	I	II	III	IV	V
CCA	74	—	—	—	1
ICA	39	17	12	4	3
ECA	56	8	4	4	3

Note.—I = no vascular abnormalities, II = mild stenosis (1%–30%), III = moderate stenosis (31%–70%), IV = severe stenosis (71%–99%), V = obstruction, CCA = common carotid artery, ECA = external carotid artery, ICA = internal carotid artery.

with $\bar{v}$ = mean velocity, D = inner diameter of the pipe, ρ = density (1,000 kg/m^3 for water), and η = viscosity (.001 kg s^{-1} m^{-1}). A diluted manganese chloride solution ($MnCl_2$) with the spin-lattice relaxation time of blood ($T_1 \approx 600$ ms at 1.5 T) was used for both the flowing and the stationary fluid. The radiofrequency coil used for the phantom experiments was the same as that used in the in vivo studies. At least three measurements under identical experimental conditions were performed to analyze reproducibility.

Study Group

The general suitability of the clinical protocol was first checked by pilot investigations in two young volunteers without any known vascular abnormalities. Forty-one patients, referred to our hospital suffering from carotid artery occlusive disease, were chosen from a parallel clinical trial on the evaluation of the diagnostic potential of MRA (25,26). In addition to this protocol, comparing intra-arterial DSA with time-of-flight MRA, a RACE measurement was performed at the time of the MRA examination of the supra-aortic arteries. The complete in vivo study, therefore, included 43 subjects, who ranged in age from 24 to 78 years (mean 57 ± 14 years) and included 27 men and 16 women. Informed written consent was obtained from all patients and volunteers after the complete examination had been fully explained.

Staging

The result of a detailed examination of the carotid arteries and their branches by five experienced radiologists was regarded as the gold standard for staging of arterial disease. Data on clinical history and the results of standardized bilateral US, DSA, and MRA investigations were available for all patients. Surgery reports were also included in the assessment of carotid stenosis in 10 patients with carotid endarterectomy. Each radiologist examined each of the patient's data with special emphasis on the intra-arterial DSA result. The common carotid artery (CCA), internal carotid artery (ICA), and external carotid artery (ECA) were assessed separately. According to the NASCET and ECST schemes (3,4) five degrees of stenosis, expressed as the maximum percentage reduction in the diameter of the relevant artery, were used for classification, defined as I = normal; II = mild stenosis (1%–30%, plaque); III = moderate stenosis (31%–70%); IV = severe stenosis (71%–99%); V = obstruction. A summary is given in Table 1. Sixteen vessels showed stenoses in more than one location (ICA + ECA: 15, CCA + ICA + ECA: 1).

MR Imaging Techniques

All measurements, both in vitro and in vivo, were carried out on a 1.5 T whole body imager (MAGNETOM, Siemens, Erlangen, Germany) with a transmit-and-receive coil, covering the head and neck. The clinical study protocol con-

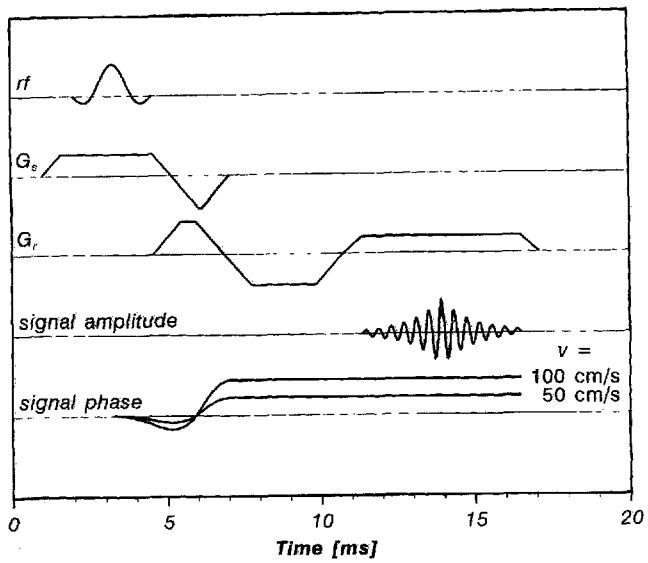

Figure 1. Schematic diagram of the RACE sequence. It combines 1D FLASH imaging with gradient motion rephasing along readout direction (x axis) and flow encoding in the direction of the slice-selection gradient (z axis). Because spatial resolution is restricted to one dimension, all signal intensity along the second direction (y axis) in the selected section is added up (summed). Evaluation of signal phases $\Phi_v(t)$ for magnetization components flowing at two different velocities $v_\perp$ is also shown.

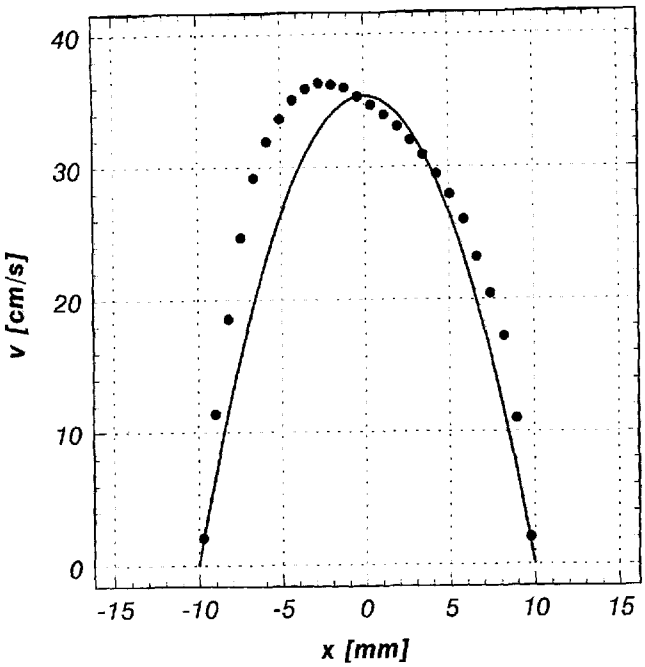

Figure 2. RACE velocity profile obtained in a phantom experiment of water (doped with $MnCl_2$) flowing through a 20-mm diameter tube at a Reynolds number (Re) of 3500 and theoretical parabolic velocity profile associated with Hagen-Poiseuille flow.

sisted of the following steps: axial and sagittal scout views were recorded to determine the exact position of the carotid bifurcation. This procedure ensured that the site of analysis was the same in all subjects. Flow quantification in the CCA was then performed during breath-hold with axial slice orientation 20 mm proximal to the bifurcation. At this position, no angular correction is required, because the vessels are nearly parallel to the z axis. A schematic diagram of the RACE sequence is shown in Figure 1. The readout gradient (G_r) is motionally nulled for both stationary and constant-velocity isochromats. During the slice-selection period (G_s), through-plane flow leads to a phase shift Φ_v of the gradient-recalled echo, depending on the velocity component $v_\perp$ perpendicular to the selected slice:

$$\Phi_v(TE) = -\gamma \int_{t_0}^{TE} v_\perp \cdot G_s \cdot (t - t_0)\, dt. \qquad (2)$$

Sequence parameters were as follows: TR = 30 ms; TE = 10 ms; 90° flip angle to increase the contrast of stationary matter; 3 mm slice thickness; 200 mm field of view with 256 frequency-encoding steps (.78 mm spatial resolution); 256 measurements with a total acquisition time of 15 s. With the chosen slice-selection gradient amplitude, $G_s \approx 4$ mT/m, the expected phase shift at a velocity $v_\perp = 1$ m/s is $\Phi_v \approx 200°$, according to Equation (2). Application of an additional saturation pulse (not shown in Fig. 1), cranial to the selected slice, was used to minimize signal contributions from venous flow. However, partial overlap of projections from different arteries may occur because of the omission of two-dimensional (2D) spatial resolution. In such cases, two or more RACE images acquired at different directions of the readout gradient are necessary. In practice, arterial overlap did not occur at our slice position, at which only few vessels are found, and a single RACE experiment (sagittal readout direction) sufficed to obtain projections, which were free from unwanted interferences. Additional rapid 2D fast low-angle shot (FLASH) imaging (TR = 31 ms; TE = 10 ms; 40° flip angle; 256 × 256 matrix) during breath-hold with identical slice parameters enabled an unambiguous assignment of the vessels of interest in the projective RACE image.

Data Processing and Analysis

After 1D Fourier transformation, the resulting series of 1D projections were transferred to a personal computer for further postprocessing.

Aliasing correction.—Because only phase shifts $\Phi_v \in (-180°, 180°]$ can be measured unambiguously, aliasing artifacts are visible in the obtained gray scale RACE images as an abrupt brightness shift, whenever $|\Phi_v| > 180°$ occurs. Such phase leaps were corrected by proper addition of a phase increment of 360°, assuming that the phase shift did not alias more than 360°. Regarding the expected velocities in the CCA and the employed gradient calibration, this assumption is normally fulfilled.

Base line correction.—In addition to motion in the presence of the flow-encoding gradient G_s, other processes, such as magnetic field inhomogeneities, gradient imperfections, eddy currents, or intrinsic effects like susceptibility variations and chemical shift differences, lead to additional spurious phase offsets in the resulting RACE images. Therefore, a base line correction procedure was necessary to extract the true flow-related phase shift. Reproducible results were obtained routinely with a cubic spline interpolation algorithm, based on the detected phase outside the arteries. However, vessels were not selected for the final analysis in cases of strong artifacts (eg, due to dental prothesis).

Flow quantification.—With the calibration result from the phantom experiments, the momentary flow velocities $v_i(t)$ as a function of time were calculated according to Equation (2) at each position. For each temporal increment, volume flow rates were determined from these spatial velocity profiles by numerical integration over all projections i inside a vessel. On the assumption of radial symmetry, $\dot{V}(t)$ is given by

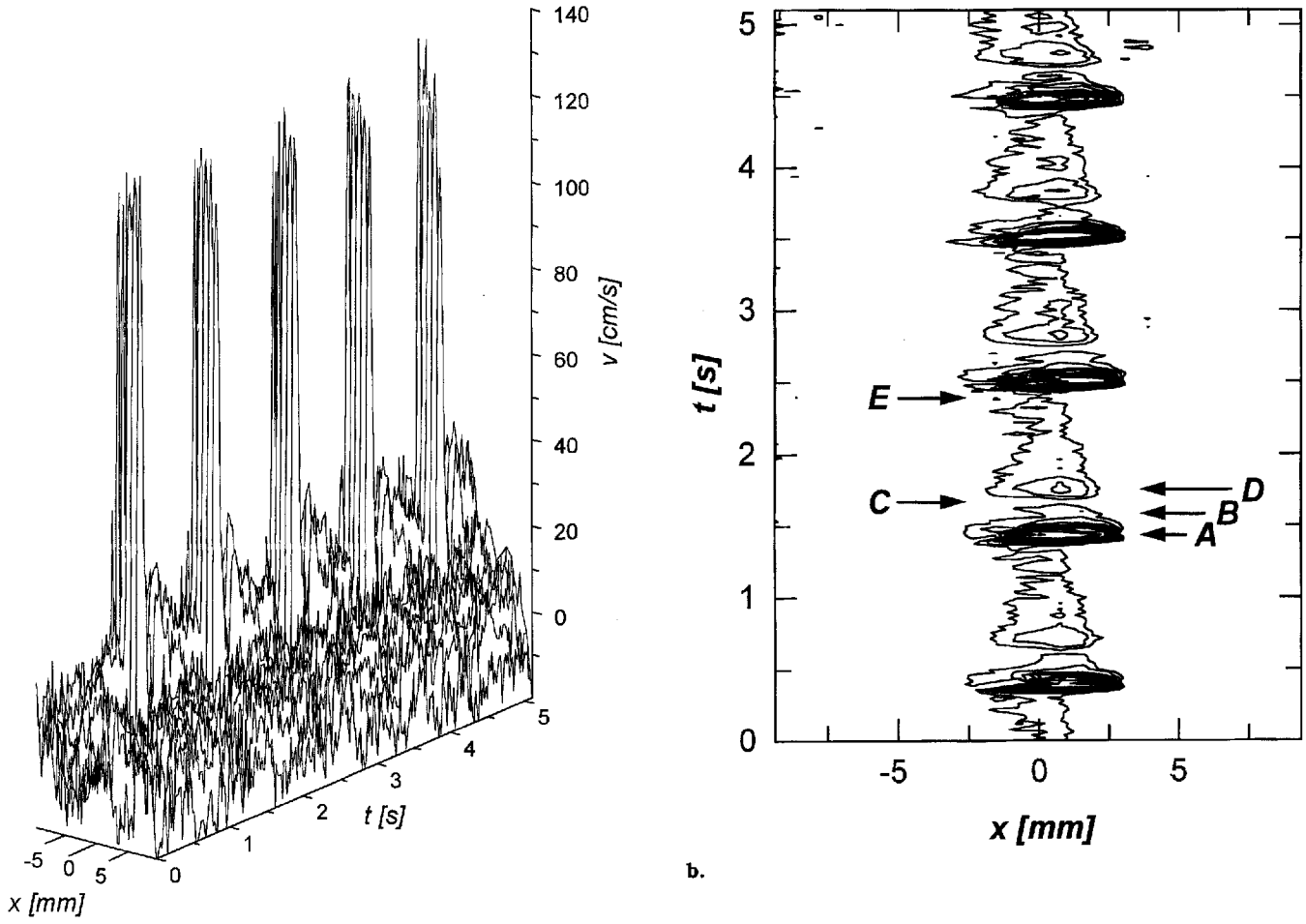

Figure 3. One-dimensional profile of the blood flow velocity through the CCA, measured with RACE in a 24-year-old male volunteer as a function of time in **(a)** three-dimensional and **(b)** contour representation. The experimental spatial resolution clearly enables the detection of an enlargement of the vessel lumen in systole. The time-dependent velocity waveforms are characterized by a double peak in systole (*A*, *B*), a sharp minimum after end systole (*C*), one flat wave in early diastole (*D*), and a minimum after end diastole (*E*).

$$\dot{V}(t) = \sum_{i=1}^{N} v_i(t)\ \pi\ r_i \delta r, \tag{3}$$

where r_i represents the distance from the center of the vessel at the position of the *i*th pixel, δr represents the spatial resolution (.78 mm in this study), and N represents the number of pixels inside the vessel. In addition to the momentary values time-averaged velocities $\langle v \rangle$ and flow rates $\langle \dot{V} \rangle$ were calculated for each heartbeat interval.

Qualitative flow pattern analysis.—In addition to changes in the velocity data, disease in the arterial system may lead to a modification of the flow waveform. Therefore, flow pattern analysis was also performed on a qualitative level by visual assessment of the temporal waveforms by two independent observers, who did not belong to the group of radiologists defining the gold standard. The observers were blinded to the gold standard data and to the quantitative RACE results. The classification depended on the degree of resolution of the following characteristic features of a normal CCA flow pattern: a double peak in systole (*A*, *B*), a sharp minimum after end systole (*C*), one flat wave in early diastole (*D*), and a minimum after end diastole (*E*). Three different types were defined (cf. Fig. 5): R1 = well resolved normal flow pattern; R2 = moderate deviations from a normal flow pattern (at least four of the characteristics *A–E* could be identified but with limited resolution due to a broadened profile); R3 = completely abnormal flow pattern (several characteristics could not be identified unequivocally). When interobserver discrepancies occurred, the higher degree of abnormalities was accepted for the final classification of the flow pattern.

Semiquantitative flow pattern analysis.—A simple system of quantifying changes of the shape of the sonogram waveforms has been suggested by Gosling (27,28). Such techniques were adopted to extract further physiological information on the arterial wall structure from the MR-detected flow curves. For this purpose, two additional parameters, the pulsatility index *PI* and the *A/B*-ratio, were calculated according to:

$$\mathrm{PI} \equiv \frac{\dot{V}_A - \dot{V}_E}{\langle \dot{V} \rangle}, \tag{4}$$

$$\mathrm{A/B} \equiv \frac{\dot{V}_A}{\dot{V}_B}. \tag{5}$$

$\dot{V}_A$, $\dot{V}_B$, and $\dot{V}_E$ represent the volume flow rates of the systolic double peak and the late diastolic minimum (compare the corresponding points *A*, *B*, and *E* of the flow waveform in Figure 5a).

Statistical analysis.—Depending on the degree of carotid artery stenosis based on the defined gold standard

(Table 1), the vessels were separated into three categories yielding numbers of cases large enough to analyze statistically: G1 = no narrowing in any of the branches, ie, classification I for CCA, ICA, and ECA (36 cases); G2 = mild or moderate stenosis (ie, classification II or III) in at least one of the branches (27 cases); G3 = severe stenosis or obstruction (ie, classification IV or V) in one or more of the branches (12 cases). To determine criteria for detecting stenoses, the RACE data were then retrospectively compared to the gold standard data. Statistical analysis was performed with the Student *t* test to compare $\langle v \rangle$, v_{peak}, $\langle \dot{V} \rangle$, *PI*, and *A/B* values between pairs of groups. In addition, analysis of variance (ANOVA) was used to test for significant differences between all three groups. All values were expressed as the mean value plus or minus one standard deviation. A *P* value less than .05 was considered statistically significant. Spearman rank correlation analysis was performed to analyze the age-dependence of flow parameters.

• RESULTS

MR Flow Phantom

As a first evaluation of the 1D velocity-mapping procedure, the expected Hagen-Poiseuille velocity profile across a 20-mm-diameter tube, through which a Newtonian fluid (water) was traveling under laminar flow conditions, was calculated according to

$$v_i(t) = \frac{8\ \dot{V}(t)}{\pi\ D^2}\left[1 - \frac{4\ r_i^2}{D^2}\right] \qquad (6)$$

and compared with the data from the phantom experiments. An example is shown in Figure 2. Similar results were also obtained in additional studies using pipes of smaller diameters (4 mm, 10 mm, and 16 mm) or glycerol/water mixtures, to adopt the viscosity of blood. Although the occurrence of turbulence in a straight, smooth-walled tube can be predicted for Reynolds numbers greater than 2,100, the assumption of parabolic velocity profiles was a good approximation in all experiments with Reynolds numbers less than 8,500. At high Reynolds numbers (Re > 8,500), reliable flow quantification was no longer possible because of the increasing importance of velocity components transverse to the main direction.

The calculated phase shift according to Equation (2) was close to the theoretical value (Φ_v = 205.1° ± 2.2° at a velocity $v_\perp$ = 1 m/s). Using this calibration, the standard deviation of the experimental flow velocities from the theoretical profile was ± .065 m/s. Volume flow rates, determined from the phase images by applying Equation (3), agreed with the values measured with the flowmeters within ± 6%. Although the mean deviation between measurement and calculation is small overall, Figure 2 shows a shifted peak of the experimental data to the left as compared with the theoretical prediction. This difference was reproducibly observed in repeated measurements for all Reynolds numbers less than 8,500 and, therefore, may be indicative of a slightly curved tube.

In Vivo Studies

All in vivo measurements were routinely performed uneventfully, taking less than 5 minutes per patient inclusive of preparation periods. Flow patterns of 75 of 86 vessels (ie, 87%) were obtained with an acceptable quality and were included in the data for subsequent analysis. A typical example of a 1D velocity map, measured as a function of time in a healthy volunteer, is shown in Figure 3. The region of the CCA can be identified easily. Within

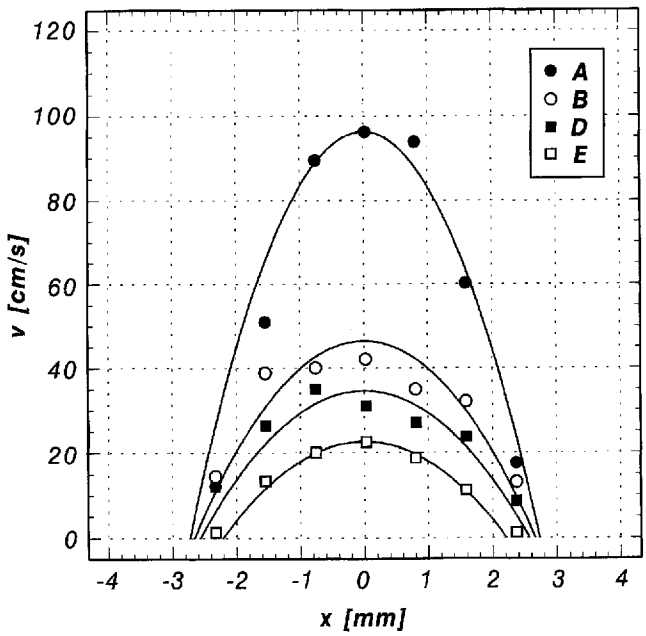

Figure 4. Comparison of spatial flow velocity profiles in the CCA, measured with RACE in a healthy male subject aged 42 years, with calculations based on a parabolic configuration. Results obtained at four different times (*A*, *B*, *D*, and *E*, cf. Fig. 3b) during the cardiac cycle are shown.

the experimental accuracy, the spatial flow velocity profiles were more nearly parabolic than blunt during the complete heartbeat interval (Fig. 4). Examples of time-dependent volume flow rates obtained from the numerical integration of the velocity projections according to Equation (3) are shown in Figure 5.

Mean values of CCA flow parameters obtained from the 36 normal vessels (ie, classification I respectively G1) were $\langle v \rangle$ = 12.2 ± 6.0 cm/s, v_{peak} = 51 ± 33 cm/s (peak systolic flow velocity), and $\langle \dot{V} \rangle$ = 4.3 ± 2.0 ml/s. Although there was a trend of reduced values in older subjects, correlation coefficients against age showed no significant association with flow. However, there was age dependence in the shape of the flow curves, leading to significant reductions of the pulsatility index *PI* and the *A/B*-ratio (*P* = .02, respectively; $P < .001$, Spearman rank correlation analysis). Graphical presentations are shown in Figure 6.

Table 2 summarizes the combined results of $\langle v \rangle$, v_{peak}, and $\langle \dot{V} \rangle$ obtained for different degrees of carotid stenosis. When compared to normal vessels (G1) employing *t* tests, no differences were seen between arteries with mild or moderate narrowing (G2), whereas all three parameters decreased significantly in cases of high-grade lesions (G3): $\langle v \rangle$, P = .002; v_{peak}, P = .002; $\langle \dot{V} \rangle$, $P < .001$). ANOVA indicated significant differences in all three velocity parameters between categories G1 and G3 as well as between G2 and G3 ($\langle v \rangle$, P = .01; v_{peak}, .01; $\langle \dot{V} \rangle$, P = .002). These results suggest that flow data may be used to separate stenoses less than 70% (ie, G1 plus G2) from greater ones (G3). Although similar trends were obtained with all three parameters, $\langle \dot{V} \rangle$ yielded the best results. Using a threshold $\langle \dot{V} \rangle^*$ = 3.0 ml/s, 11 of 12 vessels staged G3 were identified correctly on the basis of their low averaged flow rates (sensitivity: 91.7%), whereas one case of a severe ECA stenosis with $\langle \dot{V} \rangle$ = 3.7 ml/s gave a false-negative classification. In 20 cases, false-positive results were obtained (accuracy: 35.5%). From the 63 vessels without severe or subtotal stenoses, 33 were identified correctly (specificity: 52.4%). Similarly, with a velocity

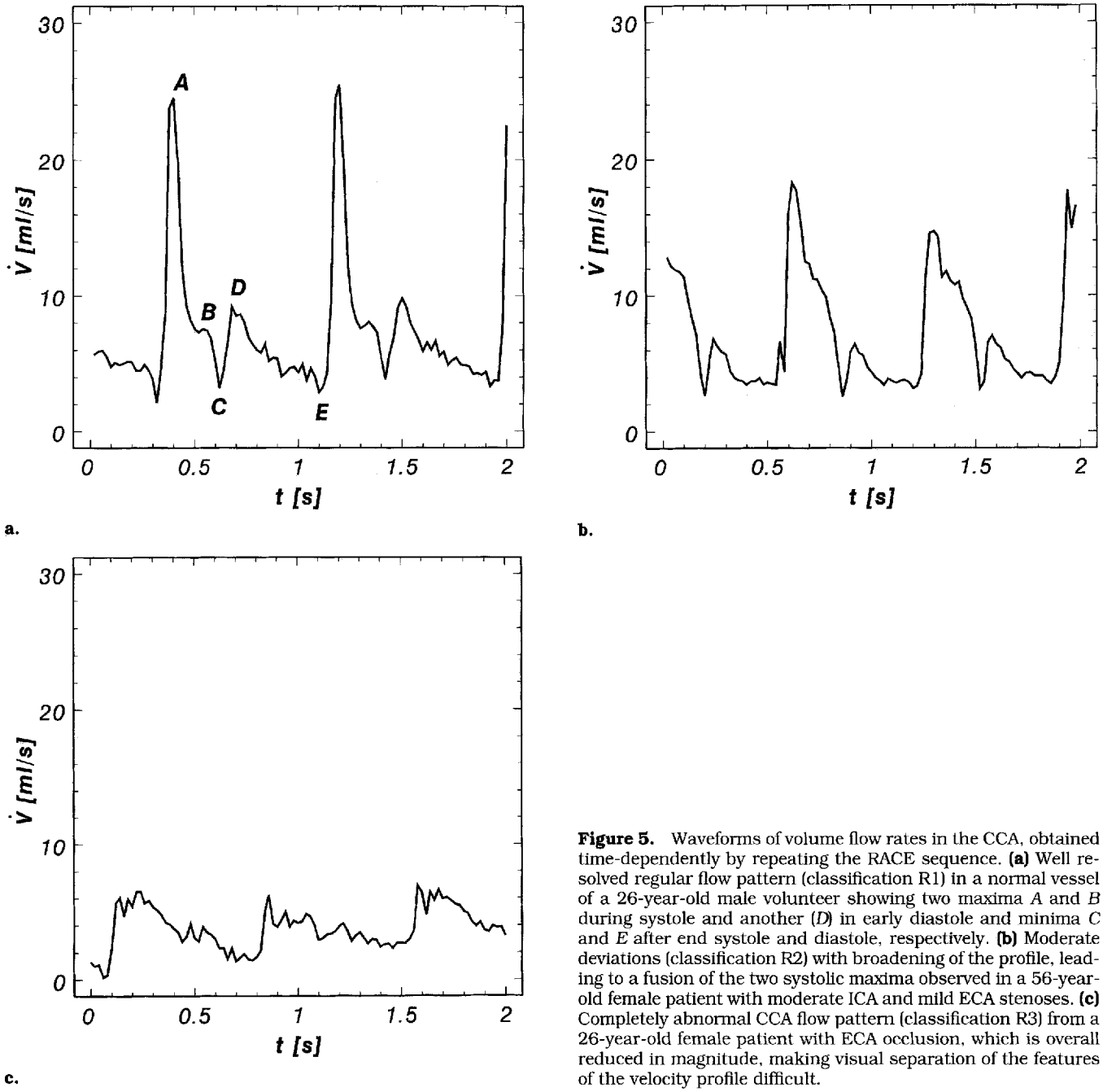

Figure 5. Waveforms of volume flow rates in the CCA, obtained time-dependently by repeating the RACE sequence. **(a)** Well resolved regular flow pattern (classification R1) in a normal vessel of a 26-year-old male volunteer showing two maxima *A* and *B* during systole and another (*D*) in early diastole and minima *C* and *E* after end systole and diastole, respectively. **(b)** Moderate deviations (classification R2) with broadening of the profile, leading to a fusion of the two systolic maxima observed in a 56-year-old female patient with moderate ICA and mild ECA stenoses. **(c)** Completely abnormal CCA flow pattern (classification R3) from a 26-year-old female patient with ECA occlusion, which is overall reduced in magnitude, making visual separation of the features of the velocity profile difficult.

threshold of $\langle v \rangle^* = 10$ cm/s, a sensitivity of 83.3%, a specificity of 55.6%, and an accuracy of 26.3% were determined.

An intraindividual comparison of blood flow through the two common carotid arteries yielded further results. In the group of normal healthy subjects (G1), no significant side difference was seen, and the observed flow ratio between right and left CCA of 1.11 ± .32 was consistent with earlier US findings (29,30). However, a significant difference was obtained in patients with unilateral high-grade stenoses (G3). In these cases ($n = 7$), the mean flow ratio between the normal and the affected side was 2.06 ± .97.

Table 2 also shows mean values of the indices *PI* and *A/B*. Although both decreased in stenosed arteries, a combined analysis of velocity data and these indices did not improve specificity or accuracy. Better results were obtained from the qualitative analysis of the complete flow patterns, assuming that diameter reductions below 70% (G2, $n = 27$) should lead to moderate deviations (R2), whereas severe stenoses or occlusions (G3, $n = 12$) should produce marked abnormalities (R3). Typical examples are presented in Figure 5. In the group of 36 unaffected vessels (G1), there was a clear trend of overestimation of deviations from a regular flow pattern, and only 50% were assessed as normal (ie, R1). However, the amount of correctly interpreted flow patterns increased to 77.7% in the group of mild or moderate stenoses and to 83.3% in patients with high grade narrowing. A summary is given in Table 3.

In addition to volume flow rates below the empirical threshold of $\langle \dot{V} \rangle^* = 3.0$ ml/s, marked deviations from the regular age-dependent flow pattern (R3) were therefore another characteristic feature indicating a diameter reduction of more than 70%. Combining both parameters for the diagnosis of occlusive carotid disease, correct staging was achieved in 69 cases (59 subcritical and 10 severe stenoses), overestimation was achieved in four,

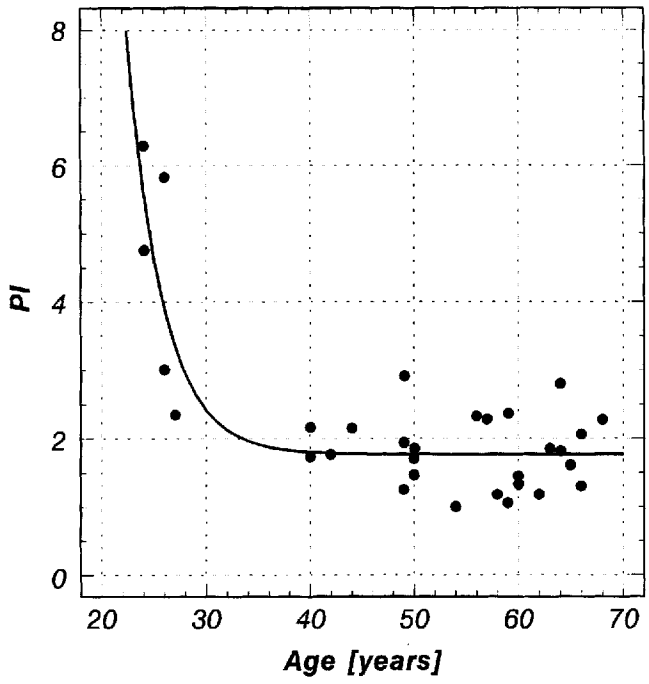

a.

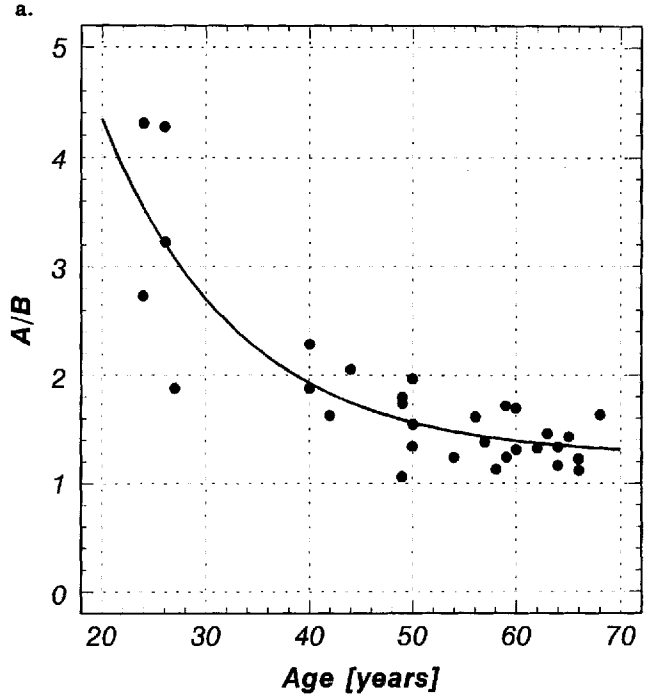

b.

Figure 6. Age-dependency of **(a)** the pulsatility index *PI* and **(b)** the *A/B*-ratio, measured in the CCA of subjects without vascular abnormalities (ie, classification I respectively G1). The solid lines show results obtained by fitting empirical functions $f = a \exp(-b \times \text{age}) + c$ to the experimental data (correlation coefficients: $R^2_{PI} = .72$ respectively $R^2_{A/B} = .74$).

and underestimation was achieved in two (sensitivity: 83.3%, specificity 93.7%, accuracy: 71.4%; Table 4).

• DISCUSSION

Characteristics of blood flow through the human carotid arteries are not simple because of the complex geometry of the bifurcation, the pulsatile nature of the flow, the distensibility of the arterial wall, and the non-Newtonian behavior of blood. However, it can be shown that (*a*) the upstream influence of flow branching is negligible, (*b*) the spatial velocity profiles are not strongly affected by assuming rigid walls in cases of unbranched vessels, and (*c*) effects of non-Newtonian rheology are of only minor consequence to the velocity field in the CCA (31). Moreover, the CCA experience a relatively constant forward flow during diastole, which occupies approximately two-thirds of the cardiac cycle. Therefore, steady flow patterns obtained with a rigid phantom of simple geometry provide a sufficient basis for a rough estimation of the maximum range of Reynolds numbers, which can be investigated using the RACE technique in straight vessel segments. The results from the phantom experiments, showing that accurate quantification of velocities is possible even at Reynolds numbers well above the usual threshold of the onset of turbulence, are consistent with findings from Evans et al, who observed no decrease in gradient echo signal intensity under comparable experimental conditions (32). The typical range of representative physiological Reynolds numbers in the CCA with a peak value around 1,200 in systole (31) is therefore sufficiently covered by the RACE technique.

Normal Carotid Hemodynamics

The observation of nearly parabolic spatial velocity profiles in healthy subjects over much of the cardiac cycle is consistent with theoretical fluid dynamic investigations (33) and in vivo pulsed Doppler studies (31,34,35). In addition, time-dependent RACE measurements provide online information about arterial wall displacements during the cardiac cycle, thus giving insight into the distensibility of the vessels. A maximum change in diameter of the CCA in volunteers of 1.0 mm is obtained from Figs. 3b and 4. Regarding the spatial resolution of our experiment, this value agrees with earlier Doppler results of .6 mm, typically found in young healthy subjects (35).

Although the RACE technique yields most of the blood flow information observer-independently, the quantitative results summarized in Table 2 showed a marked interindividual variability, even in the group of normal subjects. Two sources of this variation may be discussed. Careful analysis of the in vivo reproducibility of the estimated flow velocities yielded a random error component of ± 17%. This was below the accuracy of the phantom experiments, in which susceptibility variations and thus base line errors were less pronounced. However, in addition to such technical limitations, the patient can be expected to be the greatest source of spread among the data, because (*a*) the cardiac output can vary over a considerable range with posture and exercise, (*b*) cerebral blood flow is suspected to depend on age or body weight, and (*c*) several authors have shown that CCA blood flow varies directly with the amount of inspired carbon dioxide (29,30,36). The last factor may be important for investigations of anxious subjects.

The mean velocities and volume flow rates in the normal CCA shown in Table 2 agree with earlier MR results of 11.02 cm/s and 4.1 ml/s (37), respectively 4.9 to 7.4 ml/s (38) from single case investigations of young healthy volunteers employing phase contrast MRA or phase mapping. A summary of corresponding data from 12 Doppler US studies was given by Ackroyd et al with flow rates ranging from 5.4 to 8.3 ml/s (30). Examples of literature data of the peak systolic velocities in the normal CCA, measured with Doppler US, are 60 to 120 cm/s (39) or 59 to 147 cm/s (40). Although the highest flow rates (upper quartile: 5.5 to 9.8 ml/s) and peak velocities (upper quartile: 67 to 162 cm/s) obtained with the RACE technique fall into these ranges, the lower mean values

Table 2
Comparison of Mean Values Plus/Minus One Standard Deviation of Quantitative Blood Flow Data and Indices Describing Flow Waveforms, Measured in the Common Carotid Arteries of Subjects with Different Grades of Luminal Narrowing in the Region of the Bifurcation

	G1 (n = 36)	G2 (n = 27)	P	G3 (n = 12)	P
$\langle v \rangle$ [cm/s]	12.2 ± 6.0	11.7 ± 6.3	n.s.	6.3 ± 3.7	.002
v_{peak} [cm/s]	51 ± 33	47 ± 27	n.s.	25 ± 17	.002
$\langle \dot{V} \rangle$ [ml/s]	4.3 ± 2.0	4.1 ± 2.2	n.s.	1.89 ± .96	<.001
PI	2.2 ± 1.3	1.72 ± .41	n.s.	1.98 ± .51	n.s.
A/B	1.78 ± .80	1.39 ± .38	n.s.	1.38 ± .20	n.s.

Note.—*A/B* = *A/B* Ratio, G1 = no narrowing, G2 = mild or moderate stenosis, G3 = severe stenosis or obstruction, n.s. = not significant, *PI* = pulsatility index, v_{peak} = peak systolic flow velocity, $\langle v \rangle$ = flow velocity averaged over the cardiac cycle, $\langle \dot{V} \rangle$ = volume flow rate averaged over the cardiac cycle.

of 4.3 ± 2.0 ml/s respectively 51 ± 33 cm/s may be regarded as an indication of some systematic error associated with the method. A detailed discussion of factors affecting the accuracy of phase velocity mapping techniques was given by Firmin et al (41). Generally, an underestimation of velocities occurs in cases of improper alignment between the directions of flow and its encoding gradient G_s. However, even a misalignment of as much as 20° would produce only a 6% error. Under in vivo conditions, insufficient suppression of surrounding tissue may be another potential source of erroneously low values because of partial voluming caused by projection (42). In this case, the detected signal contains contributions from moving and stationary magnetization and will be reduced in magnitude and phase. Principally, insufficient suppression results when surrounding tissue of short T1 is present along the projection direction or, more importantly, if the effective flip angle significantly deviates from 90°. Therefore, in single cases, the position of the carotid bifurcation may have been too close to the edge of the coil, leading to an additional attenuation caused by suboptimal radiofrequency conditions.

One advantage of the use of dimensionless indices such as *PI* or *A/B* is their independence of all factors attenuating the complete flow curve. However, the observed normal ranges of both parameters show similar variations as the velocity data (Table 2). Again, this is predominantly due to a large variability among different individuals. In addition, this is superimposed by the age-dependent reduction of both parameters as demonstrated in Figure 6. Because volume flow showed only a nonsignificant trend of diminishing with increasing age, variations of cerebral blood flow cannot account for this age dependence. Other factors influencing the curves and accordingly the pulsatility index and the *A/B* Ratio are the intraluminal pressure and the arterial wall elasticity. Therefore, the observed age-dependent variations of the flow waveforms probably result from hemodynamic changes caused by a decrease in the arterial compliance and an increase in the peripheral resistance in older subjects. Identical observations are known from Doppler studies (28,43).

Staging of Carotid Artery Stenoses

Regarding the investigation of luminal narrowing, it should be emphasized that quantification of CCA blood flow does not offer any morphologic information on the carotid bifurcation but may be regarded as an indirect test of the hemodynamic significance of the degree of stenosis. Carotid stenosis is said to be hemodynamically significant when it causes a reduction in blood flow (30). Our results indicate that CCA blood flow reduction, measured as $\langle \dot{V} \rangle$ in a proximal vessel segment, does not become pronounced until luminal narrowing has reached 70%. This is consistent with intraoperative pressure gradients across the stenosis (44), intraoperative ICA flow measurements before and after endarterectomy (45), and Doppler US findings (29,30). In addition to this equivalence concerning volume flow rates, increased peak velocities v_{peak} are commonly used in sonographic studies as an indication of a severe stenosis, whereas the RACE results yielded significantly decreased values of both $\langle v \rangle$ and v_{peak}. However, this is only a fictitious contradiction. Doppler measurements are usually performed at the position of maximal luminal narrowing, leading to an acceleration of blood flow and thus high velocities, whereas our RACE data were obtained in a segment proximal to the stenosis. At this position, the vessel diameter was always unchanged, and low velocities result from the reduction of volume flow rates through the bifurcation.

Due to the above-mentioned substantial variability, even among normal subjects, the potential of human CCA blood flow data for a reliable diagnosis of small lesions must be inherently poor. It is further limited because even moderate ICA stenoses may not lead to significant reductions in CCA flow because of the capacity of the collateral ECA to accommodate to an extra flow imposed on it (45). Therefore, a sufficient differentiation between vessels staged G1 and G2 based on flow rates cannot be expected. The same holds for the relative indices and the shape of the flow curves: age-dependent alterations (eg, due to a reduced elasticity of the arterial wall) lead to modifications in the flow waveforms, which are difficult to separate from those changes produced by moderate arterial stenosis. This is, however, only of minor clinical importance. Results of NASCET and ECST demonstrated, that only in symptomatic patients with diameter reductions exceeding 70% were the risks of surgery significantly outweighed by the later benefits (3,4,46). For clinical practice, the method must therefore focus on a reliable identification of these "critical" stenoses staged G3. Our results indicate that this clinically relevant purpose may be achieved with a high sensitivity using a threshold flow rate $\langle \dot{V} \rangle^*$ = 3.0 ml/s. Reduced velocities, both $\langle v \rangle$ and v_{peak}, and large side differences in the flow results may further be used to corroborate the diagnosis.

Because most of the potential phase errors lead to an underestimation of velocities, an inherent trend of overestimation of stenosis is associated with the quantitative RACE data, ie, such errors do not reduce the sensitivity. However, additional information is necessary to eliminate false-positive results. Based on our data (Table 4), a substantial improvement of specificity and accuracy can be expected from a visual flow pattern analysis, ie, if a positive RACE result is defined as $\langle \dot{V} \rangle$ < 3.0 ml/s plus an abnormal flow curve (R3). Table 4 also shows a small de-

Table 3
Results Form a Qualitative Classification of Stenoses Based on the Assessment of the Common Carotid Artery Flow Patterns by Two Independent Observers and Comparison with the Degree of Luminal Narrowing in the Region of the Bifurcation

	G1 (n = 36)	G2 (n = 27)	G3 (n = 12)
R1	18	3	—
R2	17	21	2
R3	1	3	10

Note.—G1 = no narrowing, G2 = mild or moderate stenosis, G3 = severe stenosis or obstruction, R1 = normal flow pattern, R2 = moderate deviations from a normal flow pattern, R3 = completely abnormal flow pattern.

Table 4
RACE Detection of Hemodynamically Significant Carotid Stenoses Based on Quantitative and Qualitative Flow Parameters

Flow parameter	Sensitivity	Specificity	Accuracy
$\langle v \rangle$ < 10.0 cm/s	83.3%	55.6%	26.3%
$\langle \dot{V} \rangle$ < 3.0 ml/s	91.7%	52.4%	35.5%
$\langle \dot{V} \rangle$ < 3.0 ml/s ∧ flow pattern R3	83.3%	93.7%	71.4%

Note.—R3 = completely abnormal flow pattern.

crease in sensitivity for the combined analysis, which appears to indicate that the inherent sensitivity of the waveform analysis is somewhat lower as compared to the volume flow rates. This may be a problem if flow disturbances caused by severe disease are too distal, leading to a reduction in magnitude and thus flow rate but only to minor deviations of the features of the velocity profile at the slice position. Additional ICA and ECA flow data would be helpful in such cases. However, because of the more complicated arrangement of vessels distal to the bifurcation, a single projection is normally insufficient for a reliable estimation of flow profiles in this region (H.E. Möller and H.K. Klocke, unpublished data, 1993).

Table 4 summarizes the preliminary sensitivity/specificity/accuracy results derived retrospectively from flow parameters $\langle v \rangle$ and $\langle \dot{V} \rangle$ and from the combined qualitative/quantitative analysis of our data set. Such criteria for detecting stenoses may now serve as a base line for future estimations of sensitivity and specificity numbers in prospective studies, including subjects with a low pretest probability of disease.

• CONCLUSIONS

MR imaging of human blood flow using the 1D RACE technique was shown to have potential for providing detailed hemodynamic information in a real time single breath-hold experiment. This includes the intraluminal velocity distribution, quantification of flow rates, and vessel diameter changes during the cardiac cycle caused by vascular compliance. The reliability of the method was demonstrated both in vitro, employing sophisticated phantom experiments, and for the normal human CCA in vivo by the high degree of agreement with well established Doppler US literature data. Regarding the diagnosis of a critical stenosis (> 70%), promising results indicate additional clinical impact of MR flow quantification because these symptomatic patients can be suspected to be the primary beneficiaries of carotid endarterectomy. Owing to the short examination time, the technique is ideally suited for a combination with MRA, providing both functional and morphologic information noninvasively and observer-independently within one setting. Flow data may therefore contribute to a further reduction of false-positive MRA results. MR vascular imaging combined with blood flow quantification may also play a role as a screening technique in vascular examinations of symptomatic patients.

Acknowledgments: The authors thank Edgar Müller for his expert technical advice and Professor Werner Müller-Warmuth for assistance with the phantom development and for helpfully reviewing the manuscript.

References

1. Hahn EL. Spin echoes. Physiol Rev 1950; 80:580–594.
2. Weeden VJ, Meuli RA, Edelman RR, et al. Projective imaging of pulsatile flow with magnetic resonance. Science 1985; 230: 946–948.
3. North American Symptomatic Carotid Endarterectomy Trial Collaborators. Beneficial effect of carotid endarterectomy in symptomatic patients with high-grade carotid stenosis. N Engl J Med 1991; 325:445–453.
4. European Carotid Surgery Trialists' Collaborative Group. MRC European Carotid Surgery Trial: interim results for symptomatic patients with severe (70–99%) or with mild (0–29%) carotid stenosis. Lancet 1991; 337:1235–1243.
5. Bowen BC, Quencer RM, Margosian P, Pattany PM. MR angiography of occlusive disease of the arteries in the head and neck: current concepts. AJR 1994; 162:9–18.
6. Kido DK, Moran CJ. When should third-party payers provide reimbursement for MR angiography of the carotid arteries? AJR 1994; 162:19–20.
7. Polak JK, Kalina P, Donaldson MC, O'Leary DH, Whittemore AD, Mannick JA. Carotid endarterectomy: preoperative evaluation of candidates with combined Doppler sonography and MR angiography. Radiology 1993; 186:333–338.
8. Moran PR. A flow velocity zeugmatographic interlace for NMR imaging in humans. Magn Reson Imaging 1982; 1:197–203.
9. Ståhlberg F, Ericsson A, Nordell B, Thomsen C, Henriksen O, Persson BRR. MR imaging, flow and motion. Acta Radiol 1992; 33:179–200.
10. van Dijk P. Direct cardiac NMR imaging of heart wall and blood flow velocity. J Comput Assist Tomogr 1984; 8:429–436.
11. Bryant DJ, Payne JA, Firmin DN, Longmore DB. Measurement of flow with NMR imaging using a gradient pulse and phase difference technique. J Comput Assist Tomogr 1984; 8:588–593.
12. Young IR, Bydder GM, Payne JA. Flow measurement by the development of phase differences during slice formation in MR imaging. Magn Reson Med 1986; 3:175–179.
13. Ridgway JP, Smith MA. A technique for velocity imaging using magnetic resonance imaging. Br J Radiol 1986; 59:603–607.
14. Nayler GL, Firmin DN, Longmore DB. Blood flow imaging by cine magnetic resonance. J Comput Assist Tomogr 1986; 10: 715–722.
15. Redpath TW, Norris DG, Jones RA, Hutchison MS. A new method of NMR flow imaging. Phys Med Biol 1984; 29:891–895.
16. Feinberg A, Mark AS. Human brain motion and cerebrospinal fluid circulation demonstrated with MR velocity imaging. Radiology 1987; 163:793–799.
17. Hennig J, Müri M, Brunner P, Friedburg H. Quantitative flow measurement with the fast Fourier flow technique. Radiology 1988; 166:237–240.
18. Müller E, Laub G, Graumann R, Löffler W. RACE—real time acquisition and evaluation of pulsatile blood flow on a whole body MRI unit (abstr). In: Book of Abstracts: Society of Magnetic Resonance in Medicine 1988. Berkeley, CA: Society of Magnetic Resonance in Medicine, 1988; 729.
19. Müller E, Finelli D, Laub G. Real time quantification of blood flow on a whole body MR unit using the RACE sequence (abstr). In: Book of Abstracts: Society of Magnetic Resonance in Medicine 1989. Berkeley, CA: Society of Magnetic Resonance in Medicine, 1989; 894.
20. Engels G, Müller E, Reynen K, Wilke N, Bachmann K. Phase-mapping technique for the evaluation of aortic valve stenosis by MR. Eur Radiol 1992; 2:299–304.
21. Wacker CM, Schad LR, Gehling U, et al. The pulmonary artery acceleration time determined with the MR-RACE-technique: comparison to pulmonary artery mean pressure in 12 patients. Magn Reson Imaging 1994; 12:25–31.
22. Helzel MV, Müller E. Real-time-flow-Bestimmung der Vena cava inferior auf zwei differenten Niveaus mittels "RACE"—Pulssequenz in der MRT. Rofo Fortschr Geb Rontgenstr Neuen Bildgeb Verfahr 1993; 158:230–237.
23. Kahn T, Müller E, Lewin JS, Mödder U. MR measurement of spinal CSF flow with the RACE technique. J Comput Assist Tomogr 1992; 16:54–61.

24. Meier D, Maier S, Bösiger P. Quantitative flow measurements on phantoms and on blood vessels with MR. Magn Reson Med 1988; 8:25–34.
25. Peters PE, Bongartz G, Drews C. Magnetresonanzangiographie der hirnversorgenden Arterien. Rofo Fortschr Geb Rontgenstr Neuen Bildgeb Verfahr 1990; 152:528–533.
26. Bongartz GM, Vestring T, Drews C, Krings W, Peters PE. Effect of slice orientation in 3D magnetic resonance angiography (MRA) of the supra-aortic arteries. Eur Radiol 1991; 1:158–164.
27. Gosling RG, King DH. Arterial assessment by Doppler-shift ultrasound. Proc R Soc Med 1974; 67:447–449.
28. Gosling RG. Extraction of physiological information from spectrum-analysed Doppler-shifted continuous-wave ultrasound signals obtained non-invasively from the arterial system. In: Institute of Electrical Engineers and Medical Electronics. Monograph XXI. Stevenage, UK: Peregrinus, 1976; 73–125.
29. Uematsu S, Yang A, Preziosi TJ, Kouba R, Toung TJ. Measurement of carotid blood flow in man and its clinical application. Stroke 1983; 14:256–266.
30. Ackroyd N, Gill R, Griffiths K, Kossoff G, Appleberg M. Quantitative common carotid artery blood flow: prediction of internal carotid artery stenosis. J Vasc Surg 1986; 3:846–853.
31. Bharadvaj BK, Mabon RF, Giddens DP. Steady flow in a model of the human carotid bifurcation. Part I—flow visualization. J Biomech 1982; 15:349–362.
32. Evans AJ, Blinder RA, Herfkens RJ, et al. Effects of turbulence on signal intensity in gradient echo images. Invest Radiol 1988; 23:512–518.
33. Perktold K, Hilbert D. Numerical simulation of pulsatile flow in a carotid bifurcation model. J Biomed Eng 1986; 8:193–199.
34. Ku DN, Giddens DP, Phillips DJ, Strandness DE. Hemo- dynamics of the normal human carotid bifurcation: in vitro and in vivo studies. Ultrasound Med Biol 1985; 11:13–26.
35. Reneman RS, van Merode T, Hick P, Hoeks AP. Flow velocity patterns in and distensibility of the carotid artery bulb in subjects of various ages. Circulation 1985; 71:500–509.
36. Mattle H, Edelman RR, Reis MA, Atkinson DJ. Flow quantification in the superior sagittal sinus using magnetic resonance. Neurology 1990; 40:813–815.
37. Walker MF, Souza SP, Dumoulin CL. Quantitative flow measurement in phase contrast MR angiography. J Comput Assist Tomogr 1988; 12:304–313.
38. Bendel P, Buonocore E, Bockisch A, Besozzi MC. Blood flow in the carotid arteries: quantification by using phase-sensitive MR imaging. AJR 1989; 152:1307–1310.
39. Reneman RS, Spencer MP. Local Doppler audio spectra in normal and stenosed carotid arteries in man. Ultrasound Med Biol 1979; 8:1–11.
40. Shah KD, Nanavati PR. Realtime colour flow mapping and Doppler studies of normal carotid vertebral system. J Assoc Physicians India 1989; 37:167–171.
41. Firmin DN, Nayler GL, Kilner PJ, Longmore DB. The application of phase shifts in NMR for flow measurement. Magn Reson Med 1990; 14:230–241.
42. Peeters F, Luypaert R, Eisendrath H, Osteaux M. Time resolved flow quantification with MRI using phase methods: a linear systems approach. Magn Reson Med 1995; 33:337–354.
43. Zbornikova V, Lassvik C. Duplex scanning in presumably normal persons of different ages. Ultrasound Med Biol 1986; 12: 371–378.
44. DeWeese JA, May AG, Lipchik DO, Rob CG. Anatomic and hemodynamic correlations in carotid artery stenosis. Stroke 1970; 1:149–157.
45. Archie JP, Feldtman RW. Critical stenosis of the internal carotid artery. Surgery 1981; 89:67–72.
46. The European Carotid Surgery Trialists Collaborative Group. Risk of stroke in the distribution of an asymptomatic carotid artery. Lancet 1995; 345:209–212.